Materials Science in Semiconductor Processing 167 (2023) 107815

Contents lists available at ScienceDirect

Materials Science in Semiconductor Processing

journal homepage: www.elsevier.com/locate/mssp

An *ab initio* study on half-metallicity and lattice dynamics stability of ternary half-Heusler vanadium antimonides: *VXSb* ($X = Co$, *Rh*, and *Ir*)

Aytac Erkisi [a,*], Abdullah Candan [b]

[a] Department of Physics, Pamukkale University, Denizli, 20020, Turkey
[b] Department of Machinery and Metal Technology, Kirsehir Ahi Evran University, Kirsehir, 40100, Turkey

ARTICLE INFO

Keywords:
Half-Heusler
Half-metallicity
Ab initio calculations
Mechanical properties
Phonon

ABSTRACT

Ternary half-Heusler *VXSb* ($X = Co$, *Rh*, and *Ir*) antimonides having $C1_b$ cubic crystal structure and conforming to $F\bar{4}3m$ space group with 216 space number, have been investigated in α, β, and γ structural phases with *ab* initio simulation methods. First, the gamma phase was found to be the most favorable atomic arrangement from the enthalpies of formation and energy-volume curves calculated for these materials. Then, the electronic nature, some mechanical properties, and lattice dynamical stability were investigated in the most stable γ phase. While examining the electronic behavior of these compounds, both GGA + PBE and mBJ approaches have been used to observe the band gaps. As a result of the electronic band structure calculations, it is understood that these compounds have a half-metallic nature with 100% spin polarization. In addition, the total magnetic moments of these half-metallic ferromagnets are found to have an integer value of 1 μB per formula, which is consistent with the Slater-Pauling rule. These crystal systems have mechanical stability because the elastic constants satisfy the Born-Huang stability criteria. Besides, it has been observed that the materials exhibit ductile and anisotropic behavior. Finally, phonon dispersion curves and some thermodynamic properties for these systems were obtained and it was seen that they have lattice dynamics stability. The results obtained in this study show that these compounds are suitable candidates for spintronic applications at room temperature.

1. Introduction

The first Heusler alloy, Cu_2MnAl, was discovered by Fritz Heusler in 1903 [1]. The innovation in the discovery of the Heusler alloy is that it has ferromagnetic properties although none of its constituent elements is ferromagnetic. This has led to the opportunity to meet a very exciting new material class called Heusler compounds [2]. These materials, which draw attention with their interesting electro-magnetic, optical, and thermodynamic properties [3–11], have a huge family that includes many compounds. For many years, half-Heusler alloys, one of the members of the mentioned Heusler family, have been frequently preferred in many technological application areas such as topological insulators [12,13], spintronics [14,15], photovoltaics [16], and thermoelectrics [17,18] because of their unique physical properties.

Ternary half-Heusler alloys, which have a wide range of applications, are given with 1:1:1 stoichiometry and XYZ chemical formula, and X and Y elements are usually selected from transition metals and Z elements from the main group elements [19]. These alloys have a non-centrosymmetric cubic structure in the Structurbericht designation ($C1_b$), which is a ternary ordered variant of the CaF_2 structure matching the space group $F\bar{4}3m$ and the space number 216. Such a crystal structure can be created from the tetrahedral Zinc-Blende (*ZnS*) type structure by filling the octahedral lattice sites [20]. Moreover, such structures may have three possible different structural phases as alpha (α), beta (β), and gamma (γ) phases, depending on the atomic arrangements, which are given with Wyckoff notation in Section 3 [21,22].

Electron spin plays a dominant role in spintronics, which is a preferable device for many technological applications due to its high-spin polarization and has a remarkable effect on thermodynamic and electronic properties such as half-metallicity behavior [23–27]. In this regard, half-metallic materials, which have notable electronic characteristics, exhibit semiconductor-like behavior in one of the spin directions, whereas metallic-like behavior in the other direction in their electronic band structures [15]. To date, theoretical and experimental studies have been conducted on the electronic behavior, magneto-electronic, and thermoelectric properties of many *Co*- and *Fe*-based half-Heusler-type materials [28–35]. In particular, many

* Corresponding author.
E-mail address: aerkisi@pau.edu.tr (A. Erkisi).

https://doi.org/10.1016/j.mssp.2023.107815
Received 16 May 2023; Received in revised form 20 August 2023; Accepted 23 August 2023
Available online 29 August 2023

materials scientists have conducted intensive studies on one of these materials, *Co*-based vanadium antimonite (*CoVSb*). First, in 1963, Kripyakevich and Markiv experimentally investigated the crystal structure of this material [36], and in 1972, its ferromagnetic characteristics were reported by Terada et al. [37]. A few years later, its X-ray analysis was performed depending on pressure by Noda et al. [38]. In 1998, Kaczmarska et al. performed magnetization, Hall effect, thermopower, resistivity depending on pressure, and electron spin resonance (ESR) measurements of the related material [29]. Besides, there are impressive computational studies under density functional theory about the half-metallicity and magnetic nature of the mentioned compound using some *ab* initio methods [19,28,35,39]. Furthermore, Kong et al. examined the ductility of the same material, under low and high pressure in 2011 [31].

To the best of our knowledge, although many experimental findings and theoretical studies have been presented about the *VCoSb* compound, it has been determined that its vibrational properties, which are important for the stability of lattice dynamics, have not yet been discussed in detail. In addition, to the best of our knowledge, no theoretical or experimental study has been found about *VRhSb* and *VIrSb* systems. First, our aim in this study is to examine the phonon distribution spectra of the *VCoSb* system, which has been studied many times over the years, to complete the missing information. In addition, the secondary aim of this study is to introduce two new members (*VRhSb* and *VIrSb*) to the large half-metallic Heusler family. In addition, in this study, there are two main reasons why we chose *Rh* and *Ir* as the *X* element, apart from the *Co* element. The first reason is that elements in the same group of the periodic table often have similar electronegativity and chemical properties. These harmonious similarities are important for obtaining a good atomic bonding and a well-optimized crystal structure in the resulting new alloy. Therefore, it may be more appropriate to choose elements from the same group to minimize the instability that may occur in the lattice stability. Another reason is that elements in the same group often have similar atomic radii. This similarity in atomic radii suggests that a stable crystal structure can be formed when forming half-Heusler alloys. Thus, selection among elements with similar atomic radii can provide good structural stability by reducing the stress that may occur on the formed crystal structure.

2. Details of computations

In the presented computational work, all computations were performed with VASP (Vienna Ab initio Simulation Package) software [40–43], in which the projector-augmented wave (PAW) method [44] was used to approximate the exchange-correlation potential of the valence electrons of *V*, *Co* (*Rh* or *Ir*), and *Sb* atoms. In addition, to describe interactions between electrons, Perdew, Burke and Ernzerhof (PBE) [45] type pseudopotentials within the framework of generalized gradient approximation (GGA) have been applied. Besides, to achieve electronic band structure calculations, the modified Becke-Johnson (mBJ) exchange potential [46] of meta-Generalized Gradient Approximation (*meta*-GGA) has been employed. The valence electron configurations of the *V, Co, Rh, Ir,* and *Sb* atoms in the mentioned systems are as follows: $3d^4 4s^1$, $3d^8 4s^1$, $4d^8 5s^1$, $5d^7 6s^2$, and $5s^2 5p^3$, respectively.

During the optimization process in each structural phase, a 15 × 15 × 15 k-point mesh was automatically produced and used to sample the irreducible Brillouin zone yielding 120 k-points centered at Γ-point. Also, the kinetic energy cut-off value was chosen to be 500 eV for wave-functions. For the ionic relaxation process, the quasi-Newton method was applied, and the atomic positions of the atoms were completely relaxed until the force on each atom was less than 10^{-7} eV/Å. Also, the Methfessel-Paxton smearing method was used with 0.225 eV width. The successive change in the total energy has been taken less than 10^{-8} eV to solve the Kohn-Sham equations iteratively. To obtain fully relaxed atomic positions of the atoms for our systems and their well-optimized structural parameters, the relaxation process was continued until the forces and pressures on these crystal systems were minimized. Then, for the related compositions in this computational work, the electronic characteristics, lattice dynamics stabilities, and some mechanical properties were investigated using the sensitively optimized crystal structures.

3. Obtained results and discussion

At the beginning of this study, the most stable structural phase was determined among phases α, β and γ, shown three-dimensionally (3D) for these systems in Fig. 1. The unit cells of these half-Heusler structures are represented by twelve atoms for each structural phase. In addition, the Wyckoff atomic positions for the mentioned structural phases are tabulated in Table 1 [21,22]. For these systems, after obtaining the structural parameters in different atomic arrangements (*α, β,* and *γ phases*) and determining the most stable structure as *γ* phase, their elasticity properties, electronic behaviors, and lattice dynamic properties were investigated in the related stable phase.

3.1. Structural Stability and some parameters for α, β, and γ phases

The compositions studied in this study have a $C1_b$ crystal structure conforming to $F\bar{4}3m$ space group and 216 space number. In this subsection, for *VXSb* (*X* = *Co*, *Rh,* and *Ir*) compounds, the most energetically stable structural phase is presented. First, we calculated the formation enthalpies (ΔH_f) [47] to determine the energetically most suitable phase. Formation enthalpy can tell us about the structural stability of any crystal system. In this view, when the calculated formation enthalpy value of a crystal system in any structural phase is smaller than that of others, it can be understood that it is the more energetically suitable phase. In this study, the formation enthalpies for different structural phases of the related systems were calculated according to the formula given below:

$$\Delta H_f = E_{tot} - \left(xE_A^{bulk} + yE_B^{bulk}\right) \quad (1)$$

In this formula, E_{tot} is the total energy of the unit cell of the crystal, which is given by the A_xB_y chemical formula and E_A^{bulk} and E_B^{bulk} are the ground state energies of *A* and *B* atoms in their bulk crystal form. For *α*, *β*, and *γ* structural phases of these compounds, the calculated formation enthalpies are presented in Table 2. In this table, it can be clearly seen that the *γ* structural phase is the most suitable phase for these crystal systems because the calculated formation enthalpy values for the *γ* structural phase are smaller than those of the other phases. In addition, the negative formation enthalpies indicate that the respective crystal systems can be synthesized only in the *γ* structural phase under consideration.

After the optimization processes have been performed for each different structural phase of our systems, the total energies per formula unit as a function of the volume of these compositions have been fitted to the formula (in Eq. (2)) known as the third-order Birch-Murnaghan equation of state [48] below to draw energy-volume graphs (Fig. 2). Because of the fitting process, some structural parameters such as lattice parameters, bulk modulus, and their pressure derivatives were obtained. For each system, a well-converged ground state was obtained with the asymptotic standard errors using the fitting process being smaller than approximately 1%.

$$E(V) = E_0 + \frac{9V_0B_0}{16}\left\{\left[\left(\frac{V_0}{V}\right)^{2/3} - 1\right]^3 B_0' + \left[\left(\frac{V_0}{V}\right)^{2/3} - 1\right]^2\left[6 - 4\left(\frac{V_0}{V}\right)^{2/3}\right]\right\} \quad (2)$$

In the formula given above, V_0 and V are the reference and deformed volumes, respectively. Also, B_0 is the bulk modulus and B_0' is the de-

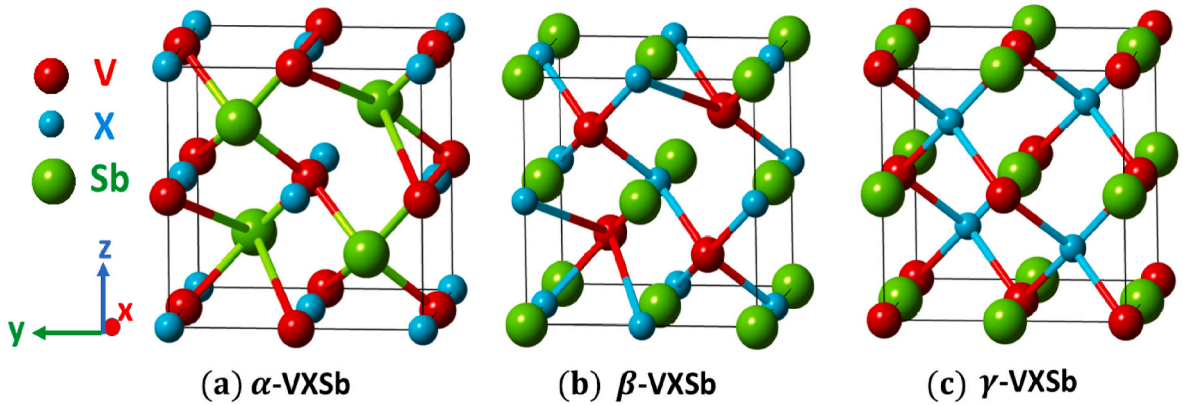

Fig. 1. The three-dimensional (3D) crystallographic shape of *VXSb* (*X* = *Co*, *Rh*, and *Ir*) half-Heusler alloys in (a) α-phase, (b) β-phase, and (c) γ-phase.

Table 1
For α, β, and γ phases, the Wyckoff notation of three atoms. The given positions are 4a:(0,0,0)a, 4b:(0.5,0.5,0.5)a, and 4c:(0.25,0.25,0.25)a, where a is the lattice constant.

Structural Phase	X	Y	Z
α	4c	4b	4a
β	4b	4a	4c
γ	4a	4c	4b

Table 2
The obtained structural parameters, calculated formation enthalpies, and bond lengths of half-Heusler vanadium-based antimonides (*VCoSb*, *VRhSb*, and *VIrSb*) for α, β, and γ phase.

Material	*Phase*	a_0 (Å)	B_0 (GPa)	$B_0^{'}$	V-X (Å)	V–Sb (Å)	ΔH_f (eV/atom)
VCoSb	α	6.017	101.7	5.25	2.61	3.01	0.331
	β	5.944	106.0	5.40	2.57	2.97	0.237
	γ	5.822	139.8	5.42	2.52	2.91	−0.248
VRhSb	α	6.151	119.4	5.06	2.66	3.08	0.111
	β	6.072	124.0	4.93	2.64	3.05	0.007
	γ	6.068	140.6	4.95	2.63	3.04	−0.282
VIrSb	α	6.142	134.6	5.03	2.66	3.07	0.287
	β	6.056	137.6	4.67	2.63	3.03	0.033
	γ	6.107	167.8	5.24	2.64	3.05	−0.278

rivative of the bulk modulus with respect to pressure. In this formula, B_0 is defined as $B_0 = -V\left(\partial P/\partial V\right)_{P=0}$ while $B_0^{'}$ is defined as $B_0^{'} = \left(\partial B/\partial P\right)_{P=0}$ and also, these parameters are generally taken from fits to experimental data.

Considering the energy-volume curves drawn separately for each structural phase of the *VXSb* (*X* = *Co*, *Rh*, and *Ir*) compounds in Fig. 2, γ phase is the most energetically optimal atomic arrangement for the respective systems. Also, for the *VCoSb* system having at the face-centered cubic $C1_b$ crystal structure in γ phase, as a result of our computations, the lattice parameter is obtained with just a 0.45% difference from the experimental result [49]. As seen in Table 2, the calculated bulk modulus in the γ phase for all compounds is greater than other phases, and the relatively high bulk modulus indicates that the mentioned crystal structures are hard materials. For the *VCoSb* system, the computed bulk modulus differs by almost 7% from the experimental results [31,50]. Also, these materials have large pressure derivatives of bulk modulus, especially in the γ phase. This situation means that these materials show strong sensitivity to the pressure changes.

Furthermore, it can be seen from Table 2 that the obtained bond lengths of *V - X* (*X* = *Co*, *Rh*, and *Ir*) and *V - Sb* are almost lower in the γ structure and this causes a decrease in the lattice parameters and ground state energies. Thus, it is understandable why these systems have lower ground state energies in the γ phase.

3.2. Electronic behaviors with magnetic moments

The electronic band structure and density of states (DOS) are usually used to describe the electronic nature of a solid crystal. As can be seen

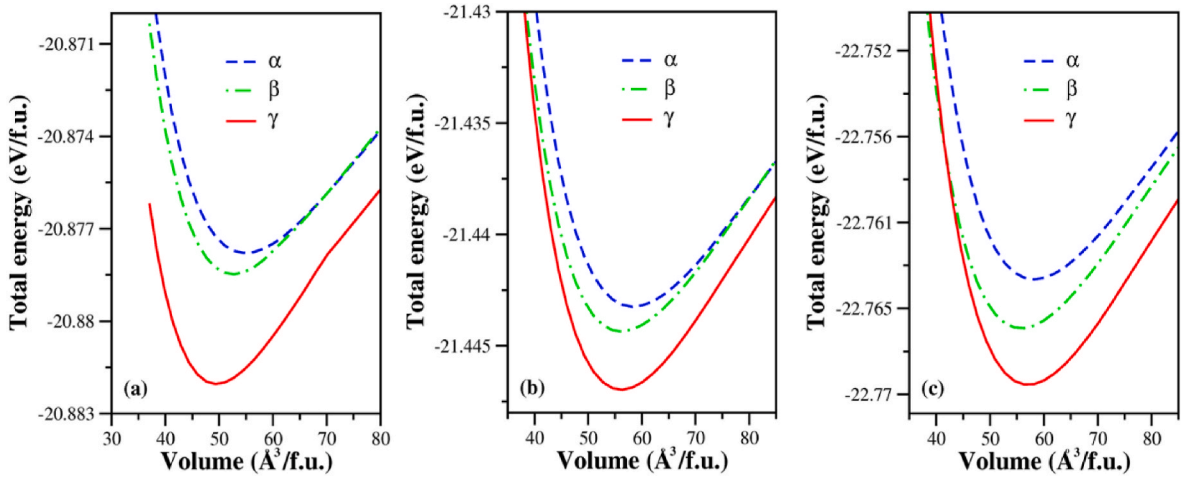

Fig. 2. Total energies as a function of unit cell volume in α, β, and γ phases of (a) *VCoSb*, (b) *VRhSb*, and (c) *VIrSb* half-Heusler compounds.

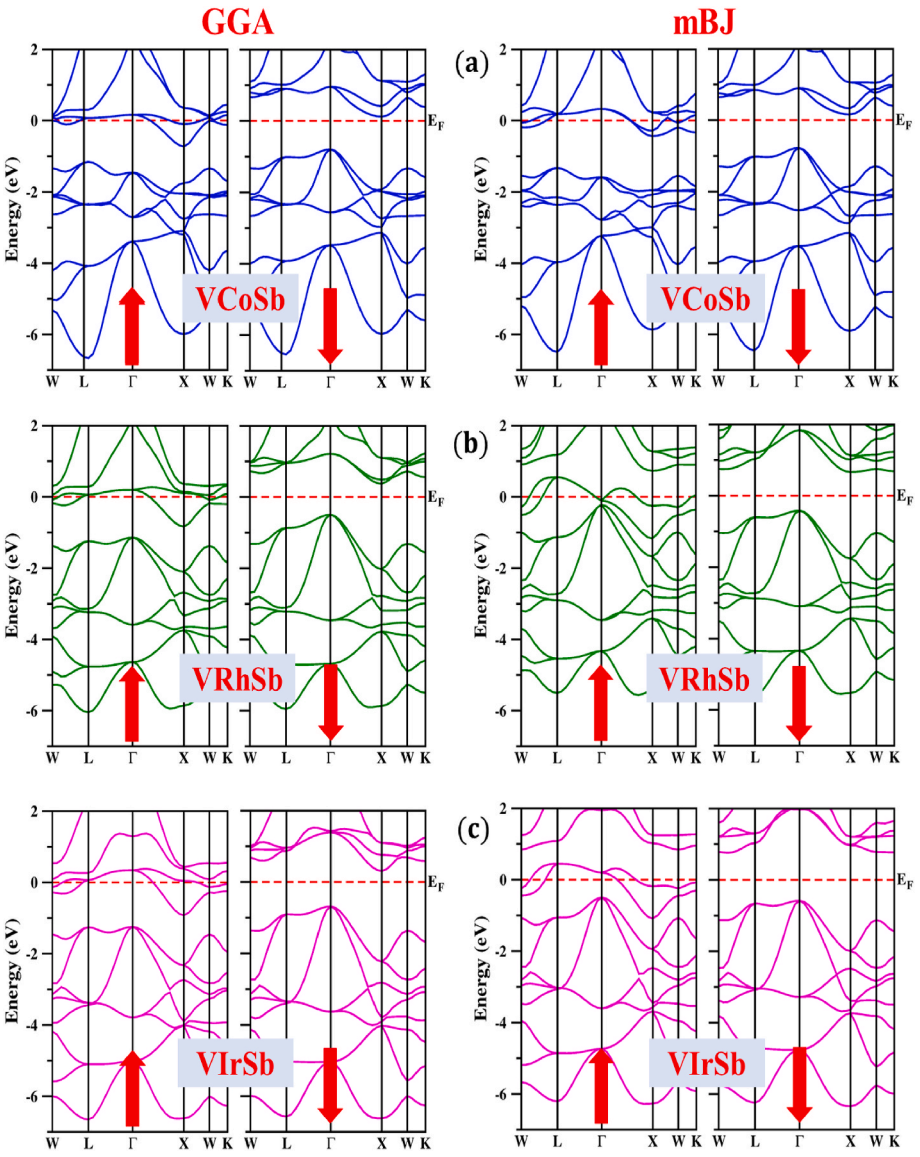

Fig. 3. The spin-polarized band structures of (a) VCoSb, (b) VRhSb, and (c) VIrSb half-Heusler compounds using GGA-PBE and mBJ.

from Fig. 3, for the related vanadium antimonides (*VCoSb*, *VRhSb*, and *VIrSb*) in the stable gamma phase, using the GGA and mBJ approximations, the spin-polarized electronic band structures were calculated and separately plotted along the high symmetry lines for the first Brillouin zone. In the related graphic, it is clearly seen that all systems in this study have a half-metallic nature. In the spin-polarized electronic band structures calculated for the stable γ phase of our systems, there are indirect band gaps (Γ to X) in the minority spin channels, whereas band gaps are not seen in the majority spin channels. For the stable γ phase, the calculated band gaps in minority spin channels under the GGA and mBJ approximations are shown in Table 3. As seen in the related Table and Fig. 3, the band gaps observed under the mBJ approach are larger than those calculated using the GGA approach. The mBJ exchange potential is used to observe band gaps of wide band gap insulators with great accuracy and to improve band gaps for half-metallic materials [51, 52]. For the ternary half-Heusler *VCoSb* system, the band gap observed in the minority spin channel using the mBJ approach is in good agreement with a previous theoretical study [53]. As presented in Fig. 3, in the minority spin channels of the electronic band structures of our compounds, the valence band maximum and conduction (Γ point) band minimum (X point) are positioned on both sides of the Fermi level. Then, the monitored indirect band gaps from Γ to X point under both approximations, are as follows: 0.92 eV (GGA) and 0.94 eV (mBJ) for the *VCoSb* system, 0.87 eV (GGA) and 1.08 eV (mBJ) for the *VRhSb* system, 0.99 eV (GGA) and 1.34 eV (mBJ) for the *VIrSb* system.

The band structures of these compounds under consideration were observed to be 100% spin-polarized, which is a characteristic of half-metallic systems. It is well known that, for metallic materials, the spin polarization is usually smaller than 100% whereas half-metallics have 100%, whereas spin polarization because the density of states at the

Table 3
The calculated band gaps ($E_g = E_{min} - E_{max}$; where E_{min} is the minimum value of the conduction band and E_{max} is the maximum value of the valence band) in minority spin channels for ternary half-Heusler vanadium-based antimonides using GGA-PBE and mBJ in stable γ phase.

System	Method	E_{min} (eV)	E_{max} (eV)	E_g (eV)
VcoSb	***GGA***	0.1183	−0.7973	0.92
	mBJ	0.1609	−0.7746	0.94
VRhSb	***GGA***	0.3728	−0.4974	0.87
	mBJ	0.6643	−0.4171	1.08
VirSb	***GGA***	0.3079	−0.6828	0.99
	mBJ	0.7560	−0.5816	1.34

Fermi level in a minority spin channel is equal to zero. The spin polarization (P) can be calculated as given in the following formula [54]:

$$P = \frac{\rho\uparrow(E_F) - \rho\downarrow(E_F)}{\rho\uparrow(E_F) + \rho\downarrow(E_F)} \quad (3)$$

where $\rho\uparrow(E_F)$ and $\rho\downarrow(E_F)$ denote the density of states at the Fermi level for the majority and minority spin channels, respectively. It can be seen from Fig. 4 that the $\rho\downarrow(E_F)$ are equal to zero. In this context, according to the above formula, these compounds appear to have 100% spin polarization due to their half-metallic nature.

The orbital projected partial density of electronic states, calculated for the atoms that make up a crystal system, can provide information about which atom's orbital dominates the electronic nature of this material. For the stable γ phase, the calculated partial density of states of *V*, *X* (*X* = *Co*, *Rh*, and *Ir*), and *Sb* atoms in our compositions using the mBJ approach are presented in Fig. 5. In the partial DOS graphs of these systems, hybridizations have been observed between the *d* orbitals of *V* atoms and those of other transition metal atoms (*Co*, *Rh*, and *Ir*). The *s* and *p* orbitals of the atoms in the compositions have not much contribution to the half-metallic nature because they are positioned at relatively lower energies. In the majority of spin channels, particularly for *VRhSb* and *VIrSb* systems, the dominance of double-degenerated d_{e_g} states (d_{z^2} and $d_{x^2-y^2}$) of *V* atoms has been observed at the Fermi level. However, in the same spin channel, for the *VCoSb* system, *d* states (d_{e_g} and $d_{t_{2g}}$) of *V* atoms give almost the same contribution as *d*-states of *Co* atoms. Furthermore, it is seen that the *d* orbitals of *X* atoms are more dominant in the valence band below the Fermi energy level, almost between −2 eV and −3 eV. In this regard, it is obvious that the half-metallic nature of these systems results from the hybridization of the *d* states of the atoms in the compositions at the Fermi energy level.

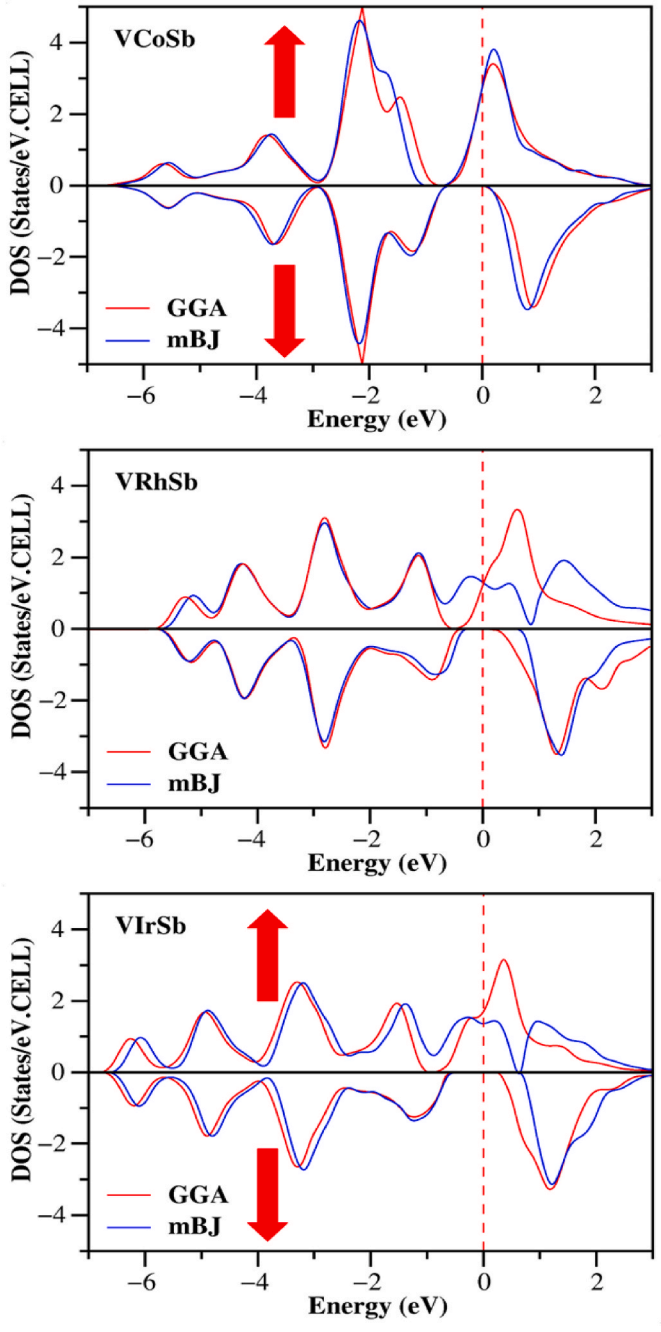

Fig. 4. The spin-polarized total and partial density of electronic states for *VXSb* (*X* = *Co*, *Rh*, and *Ir*) half-Heusler compounds using GGA-PBE and mBJ.

Due to the fact that the majority and minority spin channels in the electronic band structures are not the same, it can be concluded that the investigated materials exhibit ferromagnetic behavior in the stable γ phase. Table 4 presents the computed total magnetic moments of these systems and the partial magnetic moments of atoms. It can be seen from Table 4 that the obtained nearly integer total magnetic moments indicate half-metallicity and the partial magnetic moments of vanadium atoms play a dominant role in the ferromagnetic nature of the mentioned half-Heusler systems having half-metallic electronic behavior. In addition, the calculated total magnetic moments of our compositions appear to agree with some previous studies [19,28,35,39].

In addition, the total magnetic moments per formula unit for *VCoSb*, *VRhSb*, and *VIrSb* systems in γ phase have been calculated according to the Slater-Pauling rule for half-Heusler half-metallic ferromagnets [55,56], which is given by,

$$M_{tot} = N_v - 18 \quad (4)$$

where M_{tot} is the total magnetic moment per formula unit and N_v is the number of total valence electrons. N_v values are 19 for the mentioned crystallized solids, and it can be seen that the Slater-Pauling rule obeys well for the systems under investigation. The observed electronic and magnetic properties make these systems particularly suitable for spin-dependent electronic devices [57–60].

3.3. Mechanical stability and elasticity properties in the stable γ phase

For a solid crystal, the elastic constants (C_{ij}) are very valuable because they can be used to estimate some elasticity and thermo-elastic features, and the mechanical stability of the crystal, which is important for some technological fields such as metallurgical and materials engineering. Any crystal in cubic form has three independent elastic constants as C_{11}, C_{12}, and C_{44} [61], and these can be calculated accurately using the "stress–strain" method under *ab initio* simulations [62,63]. For *VXSb* (*X* = *Co*, *Rh*, and *Ir*) compounds in the γ phase, the calculated elastic constants and Cauchy pressures within the method are shown in Table 5. There are similarities between the calculated elastic constants for *VCoSb* in this study and those calculated by Kong et al. [31] and Shukoor et al. [64].

The mechanical stability of a crystal or its ability to resist external stresses is a desirable property for use in technological applications. In this context, whether a crystallized solid is mechanically stable depends on its elastic constants satisfying the Born-Huang criteria [65]. For crystals with a cubic structure, Born's mechanical stability criteria are given below:

$$C_{11} - C_{12} > 0;\ C_{11} + 2C_{12} > 0;\ C_{11} > 0 \text{ and } C_{44} > 0 \quad (5)$$

As seen from Table 5, the mentioned systems in the γ structural phase in the presented study are mechanically stable according to the above Born-Huang criteria. The information about the shear resistance in

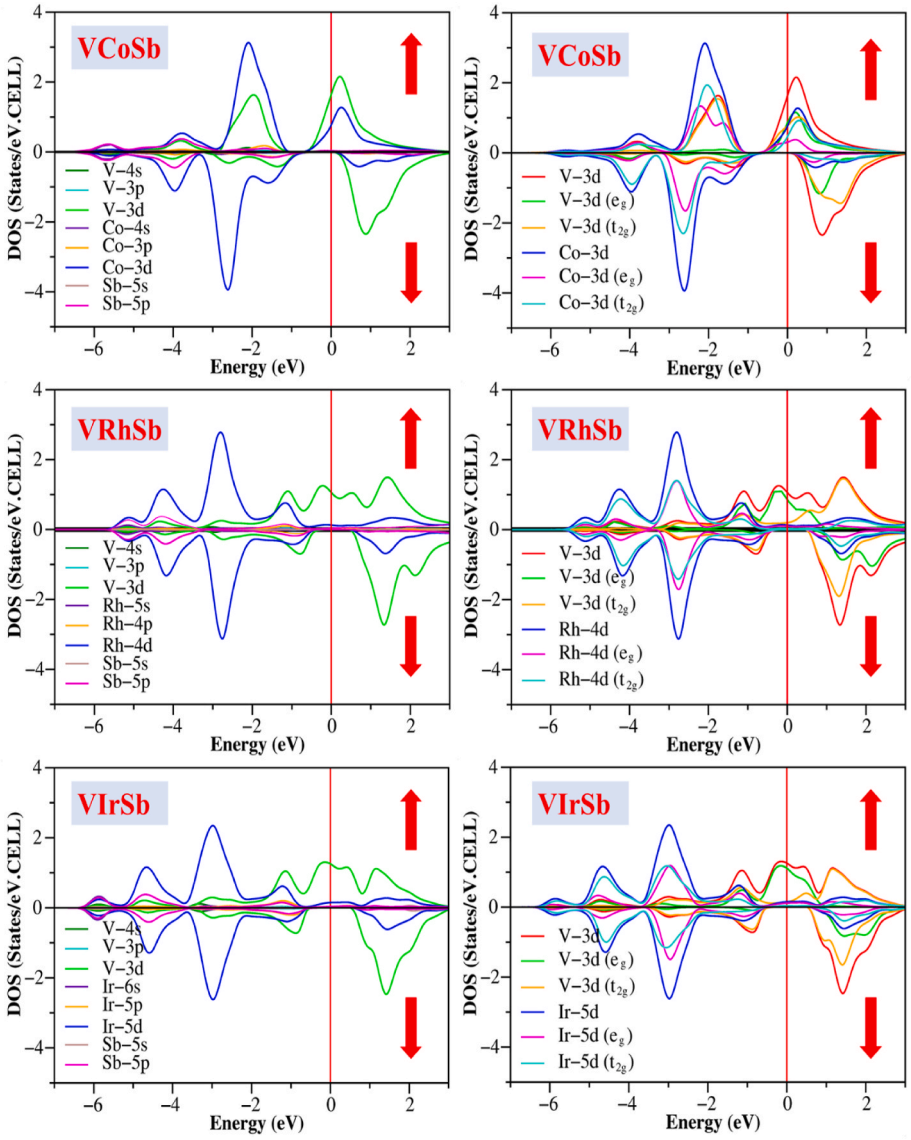

Fig. 5. The spin-polarized total and partial density of electronic states of t_{2g} and e_g for V-3d, Co-3d, Rh-4d, Ir-5d using mBJ.

Table 4
The calculated total magnetic moments of ternary half-Heusler vanadium-based antimonides for γ phase in ferromagnetic order and partial magnetic moments of *V*, *X* (*X* = *Co*, *Rh*, and *Ir*), and *Sb* atoms in systems using GGA-PBE and mBJ.

Material	Method	M_V (μ_B)	M_X (μ_B)	M_{Sb} (μ_B)	M_{tot} (μ_B)
VCoSb	***GGA***	1.155	−0.205	−0.039	1.007
	mBJ	1.131	−0.161	−0.015	1.000
VRhSb	***GGA***	1.133	−0.136	0.056	1.000
	mBJ	0.960	0.103	−0.060	1.000
VIrSb	***GGA***	1.093	−0.120	−0.036	1.001
	mBJ	0.968	0.034	−0.039	1.000

Table 5
The calculated elastic constants of *VXSb* (*X* = *Co*, *Rh,* and *Ir*) compounds in the stable γ structural phase.

Composition	C_{11} (GPa)	C_{12} (GPa)	C_{44} (GPa)	C_P (GPa)
VCoSb	225.51	80.28	49.99	30.29
VRhSb	200.19	124.01	46.79	77.22
VIrSb	224.37	130.86	103.97	26.89

[100] direction for a cubic crystallized system can be taken from the calculated C_{44} constant [66]. In our crystal systems, for the stable γ phase, the atomic bondings in [100] direction are between *V* and *Sb* atoms. It can be understood that the *V–Sb* bond in the *VIrSb* system is the strongest because the calculated C_{44} value for the *VIrSb* system is the highest. Also, the absolute value of the difference between C_{11} and C_{12} constants can give the stiffness with shear in [110] direction [67]. In the related direction for the same phase, the strongest bond belongs to the *VCoSb* system, whereas the *VRhSb* system has the weakest one.

The calculation of the Cauchy pressure ($C_P = C_{12} - C_{44}$) can be used to predict the ductility or brittleness of a solid crystal [68]. It is known that the calculated Cauchy pressure must be negative for a material with a crystalline structure to qualify as brittle; on the contrary, the Cauchy pressure should be positive for a material to be regarded as ductile. In this context, as shown in Table 5, the *Cp* values calculated for all systems in this study are positive, and therefore, they can be qualified as ductile materials. In addition, among the three systems, the most ductile material is *VRhSb,* while the ductility of the *VIrSb* system is lower than that of the others.

Besides, the calculated elastic constants can be used to predict some mechanical features of the crystallized material. Among these features, the bulk (*B*) and shear modulus (*G*) can be estimated using the relation

between the Voigt, Reuss, and Hill approximations [69–71]. As stated below in Eq. (6), the upper (B_V) and lower limits (B_R) of B for a cubic crystal are equal to each other, and the upper limit of G (G_V) and the lower limit of G (G_R) can be estimated with the help of Voigt and Reuss approximations.

$$B_V = B_R = B = (C_{11} + 2C_{12}) / 3 \tag{6}$$

$$G_V = (C_{11} - C_{12} + 3C_{44}) / 5 \tag{7}$$

$$G_R = 5(C_{11} - C_{12})C_{44} / (4C_{44} + 3C_{11} - 3C_{12}) \tag{8}$$

From the Hill approximation, the average values of the respective modules can be calculated using the formulas $B = (1/2)(B_V + B_R)$ and $G = (1/2)(G_V + G_R)$ respectively. Also, this approximation is a measure of resistance to reversible deformations upon shear stress and denotes resistance to any plastic deformation. The calculated bulk and shear modulus for our crystallized systems are presented in Table 6.

Additionally, to calculate Young's modulus (E) and Poisson's ratio (ν) of any material having a crystallized structure [72] can be used its bulk (B) and shear modulus (G) with formulas given below, respectively. These mechanical quantities calculated for the γ stable phase of the systems under investigation are given in Table 6.

$$E = (9BG) / (3B + G) \tag{9}$$

$$\nu = (3B - 2G) / [2(3B + G)] \tag{10}$$

The Young's modulus (E) of a solid crystal describes the linear strain occurring along the edges of a material under any force and can be calculated from the ratio of stress and strain. As shown in Table 6 for the *VIrSb* system, the estimated relatively higher Young's modulus indicates that this material is stiffer than the others. Also, as given in Table 6, the B/G ratios, which are usually called Pugh's ratio [73], indicate their high ductility in the γ phase, since the calculated ratios are bigger than 1.75 denote ductility, whereas smaller values indicate brittleness [73]. Accordingly, it can be assumed that the *VRhSb* system is more ductile than the others, whereas the *VIrSb* system has the lowest ductility. This result is in agreement with previous Cauchy pressure calculations.

Furthermore, it is possible to comment on whether a material is compressible by looking at the Poisson's ratio [74], which is calculated as given in Eq. (10). When the calculated Poisson's ratio of a material having a crystallized structure is approximately 0.5, it can be characterized as an incompressible one [74]. Based on the data presented in Table 6, the calculated Poisson's ratios approach a 0.3 value, which indicates that the respective systems have an almost compressible nature. Also, the related ratio can be used to determine the atomic bonding type of a solid crystal. It is well known from the literature that for covalent-type bondings, this ratio should be around 0.1, whereas the same ratio should be almost 0.25 and 0.33 for ionic-type and metallic-type bondings, respectively [75–77]. Hence, metallic-type bonding is dominant in our systems.

The shear anisotropy factors (A for the {100} planes family and A_- for the {110} planes family) depended on the crystal planes, which are among the important elasticity properties of any crystallized material, and can provide information about the degree of isotropic behavior. For crystals with a cubic structure, shear anisotropy factors can be calculated from Eq. (11) and Eq. (12) [78]. The related values calculated according to the given formulas are presented in Table 7.

Table 6
The predicted upper and lower limits, average values of bulk and shear modulus, Young's modulus, and Poisson's ratios for *VXSb* (X = *Co*, *Rh*, and *Ir*) systems in the stable γ phase.

System	B (GPa)	G_V (GPa)	G_R (GPa)	G (GPa)	B/G	E (GPa)	ν
VCoSb	128.69	59.04	57.11	58.07	2.22	151.44	0.304
VRhSb	149.40	43.31	42.87	43.09	3.47	117.94	0.368
VIrSb	162.03	81.08	69.80	75.44	2.15	195.92	0.299

Table 7
For *VXSb* (X = *Co*, *Rh*, and *Ir*) compositions in the stable γ phase, the calculated shear anisotropy factors (A and A_-), sound velocities (longitudinal (v_l), transverse (v_t), and average (v_m) wave velocities), Debye (Θ_D), and melting temperatures (T_{melt}).

System	*A*	A_-	v_l (m/s)	v_t (m/s)	v_m (m/s)	θ_D (K)	T_{melt} (K)
VCoSb	0.688	0.749	5141	2729	3050	357.09	1886
VRhSb	1.228	1.163	5025	2293	2585	290.38	1736
VIrSb	2.224	1.733	4968	2663	2973	331.82	1879

$$A = 2C_{44} / (C_{11} - C_{12}) \tag{11}$$

$$A_- = C_{44}(C_L + 2C_{12} + C_{11}) / \left(C_L C_{11} - C_{12}^2\right) \tag{12}$$

where $C_L = C_{44} + (C_{11} + C_{12})/2$.

For the crystal systems mentioned in this investigation, it can be deduced from Table 7 that the anisotropic behavior observed for {100} planes is greater than for {110} planes. Besides, it can be concluded that the *VRhSb* system is relatively more isotropic than the other two systems in the stable γ phase.

Sound conductivity, which is among the thermoelastic properties of a crystal, is one of the most important parameters to be known. In this context, there are three types of wave velocities, namely longitudinal (v_l), transverse (v_t) and average (v_m) wave velocities, which can be calculated from Navier's equations [79,80] as follows:

$$v_l = [(B + (4G/3))/\rho]^{1/2} \tag{13}$$

$$v_t = [G/\rho]^{1/2} \tag{14}$$

$$v_m = \left\{(1/3)\left[\left(2/\left(v_t^3\right)\right) + \left(1/\left(v_l^3\right)\right)\right]\right\}^{-1/3} \tag{15}$$

where ρ is the density of the material. The calculated parameters related to wave velocities for our crystal systems are given in Tables 7 and it can be seen that the sound conductivity in the *VCoSb* system is better than in other materials.

Among the other thermoelastic properties, the Debye (θ_D) and melting (T_{melt}) temperatures of a solid material are crucial parameters. Using the calculated wave velocities, the Debye temperature can be estimated from Eq. (16) [79].

$$\theta_D = (h/k)[(3n/4\pi)(N_A\rho/M)]^{1/3} v_m \tag{16}$$

In the given formula above, h and k are Planck's and Boltzmann's constants, respectively, N_A is Avogadro's number, M is the molecular weight, and n is the number of atoms in the molecule. For our systems in a crystallized face-centered cubic structure, the calculated Debye and melting temperatures are tabulated in Table 7. Table 7 shows that the calculated Debye temperature value for the *VCoSb* system (357.09 K) is higher than the others, whereas the *VRhSb* system (290.38 K) has the lowest value.

In this section, where we discuss the mechanical properties, we can finally look at how melting temperatures (T_{melt}) [81] have been predicted for our materials. This parameter is calculated using the formula given below.

$$T_{melt} = \left[553\ K + \left(\frac{5.91\ K}{GPa}\right) C_{11}\right] \pm 300\ K \tag{17}$$

As shown in Table 7, the *VCoSb* system (1886 K) has the highest value and the *VRhSb* system (1879 K) has the lowest melting temperature value obtained, which is compatible with the estimated Debye temperatures. For the *VCoSb* system in this study, it can be concluded that some mechanical and thermo-elastic parameters calculated by *ab*

initio simulation methods are approximately in agreement with previous theoretical works [31,64]. To the best of our knowledge, there is no available data in the literature to make a meaningful comparison for *VRhSb* and *VIrSb* crystal systems.

3.4. Lattice dynamical stability and thermodynamic properties

Phonons are quantized vibrational modes of a crystal lattice, and the calculation of these modes gives information about the lattice's dynamic stability and the behavior of atoms in the crystal. Therefore, the calculated vibrational modes are essential for understanding how energy is distributed throughout the crystal and for determining the thermo-elastic and mechanical properties of the crystal. In this regard, the vibrational properties of a crystal, which are described by phonons, are directly related to its mechanical and thermo-elastic properties such as elastic constants, sound velocities, and mechanical stability. This information about the mechanical properties is of vital importance in predicting the response of crystalline materials to stress, deformation, or fracture. On the other hand, the investigation of phonon properties allows the exploration and understanding of the behavior of different materials and crystal structures. Accordingly, knowing the vibrational properties of a crystalline material is important in the material design process to identify materials with desired thermal or mechanical properties, predict the stability of crystal structures, and examine the effects of crystal defects on phonon behavior. In summary, calculating the phonon modes of a material with a crystalline structure enables the thermo-elastic, optical, and mechanical properties of materials to be explored, and thus can be used in many fields such as materials science

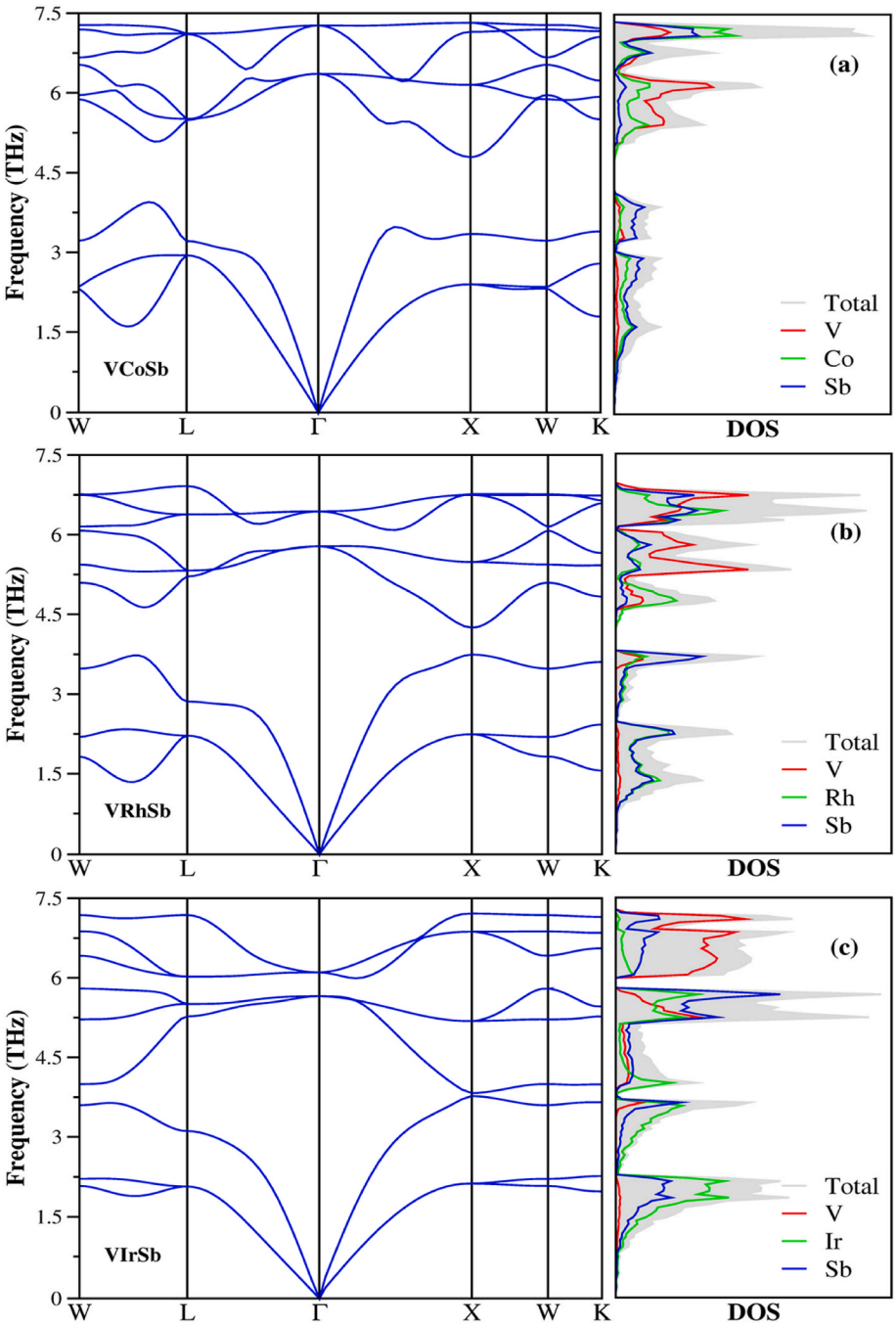

Fig. 6. The phonon dispersion curves, total and partial density of states of (a) *VCoSb*, (b) *VRhSb*, and (c) *VIrSb* half-Heusler compounds.

and engineering [82–84]. In this regard, to determine whether the ternary vanadium-based antimonides (*VCoSb*, *VRhSb*, and *VIrSb*) under investigation are lattice dynamically stable or not, the vibrational properties obtained by *ab initio* simulations have been examined. To compute the phonon frequencies depending on the interatomic force constants belonging to these systems, the PHON code [85] has been utilized, which is based on a supercell method using the finite displacement technique [86,87]. For our systems, 2 × 2 × 2 supercells were produced to obtain phonon dispersion curves plotted along the high symmetry directions in the irreducible Brillouin zone and shown in Fig. 6. Besides, in this figure, the atom projected vibrational density of states for the atoms in the mentioned crystal systems are given. As far as we searched the literature, we found that there are no studies evaluating the lattice dynamic stability of these materials; therefore, we were unable to compare our data with previously obtained data. Moreover, the fact that the lattice dynamic stability of the *VCoSb* material, which has inspired many experimental and theoretical studies, makes this study more important in terms of using this material in some technological applications.

There are four atoms in the primitive cell of each of the ternary half-Heusler *VXSb* ($X = Co, Rh$, and *Ir*) systems in this study, and as a result, a total of nine phonon branches have been obtained in the phonon spectrum distributions, as expected. As can be seen from Fig. 6, three of these branches are acoustic and six are optical. Related half-Heuslers are dynamically stable because they have no imaginary frequency, which is often called the soft mode. In particular, the phonon DOS plots for the *VRhSb* and *VIrSb* crystal systems show that the *V* atoms contribute more to higher frequencies due to their relatively smaller atomic mass than the others in these systems. In the phonon DOS graph of the *VCoSb* crystal system, it can be seen that *Co* atoms together with *V* atoms also contribute to high frequencies. In addition, these materials show clear frequency gaps between the optical and acoustic branches. In particular, for the *VCoSb* material, since the *Co* atoms are lighter than the *Rh* and *Ir* atoms, the corresponding gap is larger than other phonon dispersion curves. The observed frequency gaps are almost 0.840 THz for *VCoSb*, 0.506 THz for *VRhSb,* and 0.194 THz for *VIrSb*.

It is known that the transverse ultrasound wave velocity is given as $\left(C_{44}/\rho\right)^{1/2}$. Also, in the phonon dispersion spectra, the slope of the transverse acoustic (TA) branch $\left(d\omega/dk\right)$ for the $\Gamma - X$ direction gives the transverse ultrasound wave velocity. As seen from Fig. 6, it can be concluded that the slopes of the graphs for the *VCoSb* and *VIrSb* half-Heusler systems, show almost the same behavior. Therefore, the reason for the C_{44} constant to be different can be related to the difference in the density of the compounds, and also the atomic masses of the *Ir* (192.22 g/mol) and *Co* (58.933 g/mol) elements are different.

Furthermore, we investigated some thermodynamic properties of *VXSb* ($X = Co$, *Rh*, and *Ir*) materials within the quasi-harmonic Debye model [88] by solving the nonequilibrium Gibbs function $G^*(V;P,T)$, which can be expressed as follows:

$$G^*(V;P,T) = E(V) + PV + A_{vib}(\theta_D(V);T) \tag{18}$$

where $E(V)$ is the total energy of the bulk crystal and $A_{vib}(\theta_D(V);T)$ is the vibrational Helmholtz free energy which is known as

$$A_{vib}(\theta_D(V);T) = nkT\left[\frac{9\theta_D}{8T} + 3\ln\left(1 - e^{-(\theta_D/T)}\right) - D\left(\frac{\theta_D}{T}\right)\right] \tag{19}$$

where n and k denote the number of atoms per formula unit and Boltzmann's constant, respectively, and $D(\theta_D/T)$ is known as the Debye integral, which is given as

$$D(\theta_D/T) = \frac{3}{(\theta_D/T)^3}\int_0^{\theta_D/T}\frac{x^3}{e^x - 1} \tag{20}$$

In the above equation, θ_D represents the Debye temperature and is defined as

$$\theta_D = (\hbar/k)\left[6n\pi^2V^{1/2}\right]^{1/3} f(v)\left(\frac{B_S}{M}\right)^{1/2} \tag{21}$$

where M and v represent molecular mass per formula unit and Poisson's ratio, respectively. Also, in the related equation, $f(\sigma)$ is given below:

$$f(v) = \left\{3\left[2\left(\frac{2}{3}\frac{1+v}{1-2v}\right)^{3/2} + \left(\frac{1}{3}\frac{1+v}{1-v}\right)^{3/2}\right]^{-1}\right\}^{1/3} \tag{22}$$

In the expressions above, B_S denotes the adiabatic bulk modulus and can be approximated as,

$$B_S \approx B(V) = V\left(\frac{d^2E(V)}{dV^2}\right) \tag{23}$$

Thus, the nonequilibrium Gibbs function $G^*(V;P,T)$ depending on $V(P,T)$ can be solved as

$$\left(\frac{\partial G^*(V;P,T)}{\partial V}\right)_{P,T} = 0 \tag{24}$$

As a result, the temperature-dependent thermodynamic properties such as heat capacity at constant volume (C_V), internal energy (U), and entropy (S) can be calculated as given by respectively,

$$C_V = 3nk\left[4D\left(\frac{\theta_D}{T}\right) - \frac{3(\theta_D/T)}{e^{(\theta_D/T)} - 1}\right] \tag{25}$$

$$U_{vib} = nkT\left[\frac{9}{8}\left(\frac{\theta_D}{T}\right) + 3D\left(\frac{\theta_D}{T}\right)\right] \tag{26}$$

$$S_{vib} = nk\left[4D\left(\frac{\theta_D}{T}\right) - 3\ln\left(1 - e^{-(\theta_D/T)}\right)\right] \tag{27}$$

The plotted temperature-dependent heat capacity, internal energy, free energy, and entropy changes of these systems under given expressions [89,90] are graphically given in Fig. 7. While examining the thermodynamic properties, the temperature range was kept quite wide and was taken between 0 and 1000 K for all calculations. The heat capacity values obtained for our systems tend to rise rapidly depending on T^3 at low temperatures, then around 250 K, reaching an almost constant value called the Dulong-Petit limit. The observed heat capacities for all three systems show a similar trend with increasing temperature. In the temperature-entropy graphs, the values obtained for the *VRhSb* and *VIrSb* systems are almost the same and slightly higher than the values observed for *VCoSb*. Additionally, the entropy of all systems has increased with increasing temperature. In the temperature-internal energy and temperature-free energy graphics, the *VRhSb* and *VIrSb* systems exhibited almost the same behavior between 0 and 1000 K. Furthermore, in the observed temperature range, it was evident that the internal energy of all systems increases with temperature, on the contrary, the free energy decreases with temperature.

4. Conclusion

In this computational work, the energetically structural stability, mechanical and thermodynamic properties, electronic and magnetic behavior, and vibrational properties of ternary half-Heusler *VXSb* ($X =$ *Co*, *Rh*, and *Ir*) compounds were investigated. These solid materials have $C1_b$ cubic crystal structure and conform to $F\bar{4}3m$ space group. They have been examined in three different atomic arrangements, which are usually called α, β, and γ phases and given in Wyckoff notation during the structural stability investigation. For the systems investigated in this study, the γ phase was found to be the most thermodynamically and

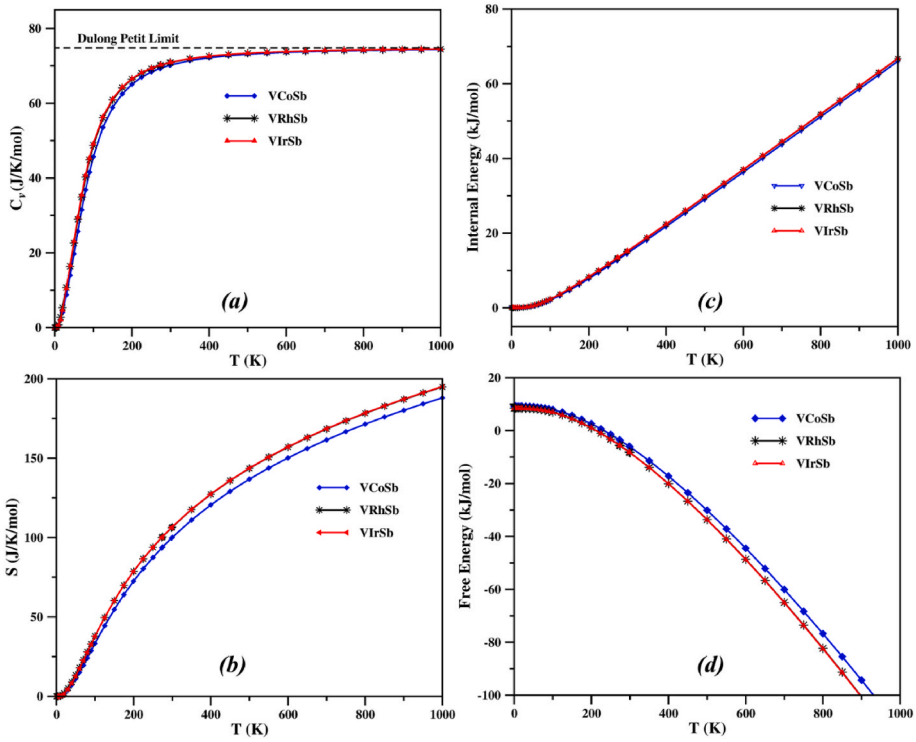

Fig. 7. (a) The specific heat capacity, **(b)** entropy, **(c)** internal energy, and **(d)** free energy versus temperature for *VXSb* (*X* = *Co*, *Rh*, and *Ir*) half-Heusler compounds.

energetically stable. Then, it was determined that the related crystal systems for the stable phase have a half-metallic electronic structure close to ferromagnetism. 100% spin-polarized electronic band structure calculations were carried out with GGA and mBJ approaches to more clearly observe the band gaps occurring in the minority spin channels. The obtained indirect band gaps in minority spin channels for the systems are as follows: 0.92 eV (GGA) and 0.94 eV (mBJ) for *VCoSb*, 0.87 eV (GGA) and 1.08 eV (mBJ) for *VRhSb*, 0.99 eV (GGA) and 1.34 eV (mBJ) for *VIrSb*. Additionally, the total magnetic moment of these compounds is 1.00 μB, which is in good agreement with the prediction from the Slater-Pauling rules. Since the elastic constants calculated by the stress-strain method fulfill the conditions given by Born-Huang, it has been observed that the related materials are mechanically stable and ductile. Furthermore, there is no anomaly behavior or softening mode in the obtained phonon dispersion spectra for these systems; therefore, it is concluded that these structures are lattice dynamically stable. The crystal systems in the present study can be good candidates for spintronics applications such as spin valves, spin injection devices, and magnetic tunnel junction applications (MTJs) because of their half-metallicity with 100% spin polarization.

CRediT authorship contribution statement

Aytac Erkisi: Writing – original draft. **Abdullah Candan:** Methodology.

Declaration of competing interest

The authors declare that they have no known competing financial interests or personal relationships that could have appeared to influence the work reported in this paper.

Data availability

Data will be made available on request.

Acknowledgments

This research was supported in part by TÜBİTAK (The Scientific & Technological Research Council of Turkey) through TR-Grid e-Infrastructure Project, part of the calculations has been carried out at the ULAKBİM Computer Center.

Notes

The authors have declared no conflict of interest and an equal contribution to this study.

References

[1] F. Heusler, W. Starck, E. Haupt, Magnetisch-chemische studien, Verhandlungen Dtsch. Phys. Ges. 5 (1903) 219–232.
[2] T. Graf, C. Felser, S.S.P. Parkin, Simple rules for the understanding of Heusler compounds, Prog. Solid State Chem. 39 (2011) 1–50, https://doi.org/10.1016/j.progsolidstchem.2011.02.001.
[3] I. Galanakis, P.H. Dederichs, Half-Metallic Alloys Fundamentals and Application, vol. 676, Springer, Berlin, 2005, pp. 1–39.
[4] J. Pierre, R.V. Skolozdra, J. Tobola, S. Kaprzyk, C. Hordequin, M.A. Koua-cou, I. Karla, R. Currat, E. Lelievre-Berna, Properties on request in semi-Heusler phases, J. Alloys Compd. 262–263 (1997) 101–107, https://doi.org/10.1016/S0925-8388(97)00337-X.
[5] J. Tobola, J. Pierre, Electronic phase diagram of the XTZ (X = Fe, Co, Ni; T = Ti, V, Zr, Nb, Mn; Z = Sn, Sb) semi-Heusler compounds, J. Alloys Compd. 296 (2000) 243–252, https://doi.org/10.1016/S0925-8388(99)00549-6.
[6] I. Galanakis, Orbital magnetism in the half-metallic Heusler alloys, Phys. Rev. B 71 (2005), 012413, https://doi.org/10.1103/PhysRevB.71.012413.
[7] L. Offernes, P. Ravindran, C.W. Seim, A. Kjekshus, Prediction of composition for stable half-Heusler phase from electronic band structure analysis, J. Alloys Compd. 458 (2008) 47–60, https://doi.org/10.1016/j.jallcom.2007.04.038.
[8] T. Block, M.J. Carey, B.A. Gurney, O. Jepsen, Band-structure calculations of the half-matallic ferromagnetism and structural stability of full- and half-Heusler phases, Phys. Rev. B 70 (2004), 205114, https://doi.org/10.1103/PhysRevB.70.205114.
[9] F.B. Mancoff, J.F. Bobo, O.E. Richter, K. Bessho, P.R. Johnson, R. Sinclair, W. D. Nix, R.L. White, B.M. Clemens, Growth and characterization of epitaxial NiMnSb/PtMnSb $C1_b$ Heusler alloy superlattices, J. Mater. Res. 14 (1999) 1560–1569, https://doi.org/10.1557/JMR.1999.0209.

[10] R.A. De Groot, F.M. Mueller, P.G. Van Engen, K.H.J. Buschow, Half-metallic ferromagnets and their magneto-optical properties, J. Appl. Phys. 55 (1984) 2151–2154, https://doi.org/10.1063/1.333593.
[11] Y. Xia, S. Bhattacharya, V. Ponnambalam, A.L. Pope, S.J. Poon, T.M. Tritt, Thermoelectric properties of semimetallic (Zr,Hf) CoSb half-Heusler phases, J. Appl. Phys. 88 (2000) 1952–1955, https://doi.org/10.1063/1.1305829.
[12] D. Xiao, Y. Yao, W. Feng, J. Wen, W. Zhu, X.Q. Chen, G.M. Stocks, Z. Zhang, Half-heusler compounds as a new class of three-dimensional topological insulators, Phys. Rev. Lett. 105 (2010), 096404, https://doi.org/10.1103/PhysRevLett.105.096404.
[13] H. Lin, L.A. Wray, Y. Xia, S. Xu, S. Jia, R.J. Cava, A. Bansil, M.Z. Hasan, Half-Heusler ternary compounds as new multifunctional experimental platforms for topological quantum phenomena, Nat. Mater. 9 (2010) 546–549, https://doi.org/10.1038/nmat2771.
[14] I. Galanakis, K. Ozdoğan, E. Şaşıoğlu, Ab initio electronic and magnetic properties of half-metallic NiCrSi and NiMnSi Heusler alloys: the role of defects and interfaces, J. Appl. Phys. 104 (2008), 083916, https://doi.org/10.1063/1.3005882.
[15] H. Luo, Z. Zhu, G. Liu, S. Xu, G. Wu, H. Liu, J. Qu, Y. Li, Ab-initio investigation of electronic properties and magnetism of half-Heusler alloys XCrAl (X=Fe Co, Ni) and NiCrZ (Z=Al, Ga, In), Phys. B Condens. Matter 403 (2008) 200–206, https://doi.org/10.1016/j.physb.2007.08.214.
[16] S. Kacimi, H. Mehnane, A. Zaoui, I-II–V and I–III–IV half-Heusler compounds for optoelectronic applications: comparative ab initio study, J. Alloys Compd. 587 (2014) 451–458, https://doi.org/10.1016/j.jallcom.2013.10.046.
[17] S. Sakurada, N. Shutoh, Effect of Ti substitution on the thermoelectric properties of (Zr, Hf)NiSn half-Heusler compounds, Appl. Phys. Lett. 86 (2005), 082105, https://doi.org/10.1063/1.1868063.
[18] G. Rogl, P. Sauerschnig, Z. Rykavets, V.V. Romaka, P. Heinrich, B. Hinterleitner, A. Grytsiv, E. Bauer, P. Rogl, (V, Nb)-doped half Heusler alloys based on {Ti, Zr, Hf}NiSn with high ZT, Acta Mater. 131 (2017) 336–348, https://doi.org/10.1016/j.actamat.2017.03.071.
[19] B.R.K. Nanda, I. Dasgupta, Electronic structure and magnetism in half-Heusler compounds, J. Phys. Condens. Matter 15 (2003) 7307. https://iopscience.iop.org/article/10.1088/0953-8984/15/43/014.
[20] J. Webster, K.R.A. Ziebeck, Alloys and compounds of d-elements with main group elements, in: Landolt-Bornstein, New Series, Group III vol. 19, Springer, Berlin, 1988, pp. 75–184.
[21] W. Huang, X. Wang, X. Chen, W. Lu, L. Damewood, C.Y. Fong, Structural and electronic properties of half-Heusler alloys PtXBi (with X=Mn, Fe, Co and Ni) calculated from first principles, J. Magn. Magn Mater. 377 (2015) 252–258, https://doi.org/10.1016/j.jmmm.2014.10.068.
[22] L. Guan-Nan, J. Ying-Jiu, First-principles study on the half-metallicity of half-Heusler alloys: XYZ (X = Mn, Ni; Y = Cr, Mn; Z = As, Sb), Chin. Phys. Lett. 26 (2009), 107101. https://iopscience.iop.org/article/10.1088/0256-307X/26/10/107101/meta.
[23] I. Galanakis, P.H. Dederichs, Slater-Pauling behavior and origin of the half-metallicity of the full-Heusler alloys, Phys. Rev. B 66 (2002), 174429, https://doi.org/10.1103/PhysRevB.66.174429.
[24] I.H. Bhat, D.C. Gupta, Magneto-electronic and thermoelectric properties of some Fe based Heusler alloys, J. Phys. Chem. Solid. 119 (2018) 251–257, https://doi.org/10.1016/j.jpcs.2018.04.008.
[25] F. Claudia, W. Lukas, C. Stanislav, H.F. Gerhard, S.P.P. Stuart, Basics and prospective of magnetic Heusler compounds, Apl. Mater. 3 (2015), 041518, https://doi.org/10.1063/1.4917387.
[26] S.A. Mir, D.C. Gupta, Exploration of uranium double perovskites Ba_2MUO_6 (M = Co, Ni) for magnetism, spintronic and thermoelectric applications, J. Magn. Magn Mater. 493 (2020), 165722, https://doi.org/10.1016/j.jmmm.2019.165722.
[27] S. Yousuf, D.C. Gupta, Insight into half-metallicity, spin-polarization and mechanical properties of $L2_1$ structured MnY_2Z (Z = Al, Si, Ga, Ge, Sn, Sb) Heusler alloys, J. Alloys Compd. 735 (2018) 1245–1252, https://doi.org/10.1016/j.jallcom.2017.11.239.
[28] S. Ishida, T. Masaki, S. Fujii, S. Asano, Theoretical predicts of half-metallic compounds with the Cl_b structure, Phys. B Condens. Matter 239 (1997) 163–166, https://doi.org/10.1016/S0921-4526(97)00401-8.
[29] K. Kaczmarska, J. Pierre, J. Beille, J. Tobola, R.V. Skolozdra, G.A. Melnik, Physical properties of the weak itinerant ferromagnet CoVSb and related semi-Heusler compounds, J. Magn. Magn Mater. 187 (1998) 210–220, https://doi.org/10.1016/S0304-8853(98)00125-5.
[30] L. Heyne, T. Igarashi, T. Kanomata, K.U. Neumann, B. Ouladdiaf, K.R.A. Ziebeck, Atomic and magnetic order in the weak ferromagnet CoVSb: is it a half-metallic ferromagnet? J. Phys. Condens. Matter 17 (2005) 4991–4999. https://iopscience.iop.org/article/10.1088/0953-8984/17/33/004.
[31] B. Kong, X.-R. Chen, J.-X. Yu, C.-L. Cai, Structural, elastic properties and pressure-induced phase transition of 'half-Heusler' alloy CoVSb, J. Alloys Compd. 509 (2011) 2611–2616, https://doi.org/10.1016/j.jallcom.2010.11.119.
[32] A. Bagheri, A. Boochani, S.R. Masharian, Huge figure of merit, half-metallic, and optical properties in n-type CoVSb heuslerene, Int. J. Thermophys. 43 (2022) 1–14, https://doi.org/10.1007/s10765-021-02962-2.
[33] B. Kong, B. Zhu, Y. Cheng, L. Zhang, Q.-X. Zeng, X.-W. Sun, Structural, mechanical, thermodynamics properties and phase transition of FeVSb, Phys. B Condens. Matter 406 (2011) 3003–3010, https://doi.org/10.1016/j.physb.2011.04.067.
[34] M. Zou, J.-F. Li, T. Kita, Thermoelectric properties of fine-grained FeVSb half-Heusler alloys tuned to p-type by substituting vanadium with titanium, J. Solid State Chem. 198 (2013) 125–130, https://doi.org/10.1016/j.jssc.2012.09.043.
[35] J. Tobola, J. Pierre, S. Kaprzyk, R.V. Skolozdra, M.A. Kouacou, Crossover from semiconductor to magnetic metal in semi-Heusler phases as a function of valence electron concentration, J. Phys. Condens. Matter 10 (1998) 1013–1032. https://iopscience.iop.org/article/10.1088/0953-8984/10/5/011.
[36] P.I. Krypyakevych, V.Y. Markiv, Crystal structures of ternary compounds in the systems Ti(V)-Fe(Co,Ni)-Sn(Sb), Dopov. Akad. Nauk. Ukr. RSR 12 (1963) 1606–1608.
[37] M. Terada, K. Endo, Y. Fujita, R. Kimura, Magnetic properties of cl_b compounds; CoVSb, CoTiSb and NiTiSb, J. Phys. Soc. Jpn. 32 (1972) 91–94, https://doi.org/10.1143/JPSJ.32.91.
[38] Y. Noda, M. Shimada, M. Koizumi, Synthesis of high-pressure phases of vanadium-cobalt-antimony (VCoSb) and vanadium-iron-antimony (VFeSb) with a dinickel-indium (Ni2In) (B82) type structure, Inorg. Chem. 18 (1979) 3244–3246, https://doi.org/10.1021/ic50201a060.
[39] I. Galanakis, P.H. Dederichs, N. Papanikolaou, Origin and properties of the gap in the half-ferromagnetic Heusler alloys, Phys. Rev. B 66 (2002), 134428, https://doi.org/10.1103/PhysRevB.66.134428.
[40] G. Kresse, J. Hafner, Ab initio molecular dynamics for liquid metals, Phys. Rev. B 47 (1993) 558–561, https://doi.org/10.1103/PhysRevB.47.558.
[41] G. Kresse, J. Furthmuller, Efficiency of ab initio total energy calculations for metals and semiconductors using a plane-wave basis set, Comput. Mater. Sci. 6 (1996) 15–50, https://doi.org/10.1016/0927-0256(96)00008-0.
[42] P. Hohenberg, W. Kohn, Inhomogeneous electron gas, Phys. Rev. 136 (1964), https://doi.org/10.1103/PhysRev.136.B864. B864–B871.
[43] W. Kohn, L.J. Sham, Self-consistent equations including exchange and correlation effects, Phys. Rev. 140 (1965), https://doi.org/10.1103/PhysRev.140.A1133. A1133–A1138.
[44] P.E. Blochl, Projector augmented-wave method, Phys. Rev. B 50 (1994) 17953–17979, https://doi.org/10.1103/PhysRevB.50.17953.
[45] J.P. Perdew, K. Burke, M. Ernzerhof, Generalized gradient approximation made simple, Phys. Rev. Lett. 77 (1996) 3865–3868, https://doi.org/10.1103/PhysRevLett.77.3865.
[46] F. Tran, P. Blaha, Accurate band gaps of semiconductors and insulators with a semilocal exchange-correlation potential, Phys. Rev. Lett. 102 (2009), 226401, https://doi.org/10.1103/PhysRevLett.102.226401.
[47] E. Zhao, Z. Wu, Electronic and mechanical properties of 5d transition metal mononitrides via first principles, J. Solid State Chem. 181 (2008) 2814–2827, https://doi.org/10.1016/j.jssc.2008.07.022.
[48] F. Birch, Finite elastic strain of cubic crystals, Phys. Rev. 71 (1947) 809–824, https://doi.org/10.1103/PhysRev.71.809.
[49] C.B.H. Evers, C.G. Richter, K. Hartjes, W. Jeitschko, Ternary transition metal antimonides and bismuthides with MgAgAs-type and filled NiAs-type structure, J. Alloys Compd. 252 (1997) 93–97, https://doi.org/10.1016/S0925-8388(96)02616-3.
[50] H.C. Kandpal, C. Felser, R. Seshadri, Covalent bonding and the nature of band gaps in some half-Heusler compounds, J. Phys. D Appl. Phys. 39 (2006) 776–785, https://doi.org/10.1088/0022-3727/39/5/S02.
[51] S.W. Fan, L.J. Ding, Z.L. Wang, K.L. Yao, Half-metallic ferromagnetism in wurtzite ScM (M=C, Si, Ge, and Sn): ab initio calculations, Appl. Phys. Lett. 102 (2013), 022404, https://doi.org/10.1063/1.4775680.
[52] S.W. Fan, J.H. Dong, L.J. Ding, Z.L. Wang, K.L. Yao, Half-metallic ferromagnetism in tetrahedrally coordinated compounds MGe (M = Ca, Sr and Ba): *Ab initio* calculations, Comput. Mater. Sci. 67 (2013) 83–87, https://doi.org/10.1016/j.commatsci.2012.08.026.
[53] M. Mokhtari, F. Dahmane, G. Benabdellah, L. Zekri, S. Benalia, N. Zekri, Theoretical study of the structural stability, electronic and magnetic properties of XVSb (X = Fe, Ni, and Co) half-Heusler compounds, Condens. Matter Phys. 21 (2018), 43705, https://doi.org/10.5488/CMP.21.43705.
[54] H.-M. Huang, S.-T. Xue, Q. Yu, R. Tong, A. Laref, Z.-D. He, Z.-W. Zhu, S.-J. Luo, First-principles calculations to investigate stability, electronic properties and anisotropy of half-metallic full Heusler alloy Co_2NbGa, Results Phys. 34 (2022), 105237, https://doi.org/10.1016/j.rinp.2022.105237.
[55] G.H. Fecher, H.C. Kandpal, S. Wurmehl, C. Felser, G. Schönhense, Slater-Pauling rule and Curie temperature of Co2-based Heusler compounds, J. Appl. Phys. 99 (2006), 08J106, https://doi.org/10.1063/1.2167629.
[56] K. Özdoğan, E. Şaşıoğlu, I. Galanakis, Slater-Pauling behavior in LiMgPdSn-type multifunctional quaternary Heusler materials: half-metallicity, spin-gapless and magneticsemiconductors, J. Appl. Phys. 113 (2013), 193903, https://doi.org/10.1063/1.4805063.
[57] B. Yildiz, A. Erkisi, G. Surucu, The spin effects on electronic, optical and mechanical properties of new ferromagnetic chalcopyrite: $YMnS_2$, Mater. Chem. Phys. 284 (2022), 126030, https://doi.org/10.1016/j.matchemphys.2022.126030.
[58] A. Gencer, O. Surucu, D. Usanmaz, R. Khenata, A. Candan, G. Surucu, Equiatomic quaternary Heusler compounds TiVFeZ (Z=Al, Si, Ge): half-metallic ferromagnetic materials, J. Alloys Compd. 883 (2021), 160869, https://doi.org/10.1016/j.jallcom.2021.160869.
[59] A. Candan, G. Uğur, Z. Charifi, H. Baaziz, M.R. Ellialtıoğlu, Electronic structure and vibrational properties in cobalt-based full-Heusler compounds: a first principle study of Co2MnX (X= Si, Ge, Al, Ga), J. Alloys Compd. 560 (2013) 215, https://doi.org/10.1016/j.jallcom.2013.01.102.
[60] M. Özduran, A. Candan, S. Akbudak, A.K. Kushwaha, A. İyigör, Structural, elastic, electronic, and magnetic properties of Si-doped Co2MnGe full-Heusler type compounds, J. Alloys Compd. 845 (2020), 155499, https://doi.org/10.1016/j.jallcom.2020.155499.
[61] A. Candan, S. Akbudak, M. Özduran, A. İyigör, An examination of the structural, electronic, elastic, vibrational and thermodynamic properties of Ru2YGa (Y= Sc, Ti

and V) Heusler alloys, Chin. J. Phys. 56 (2018) 1772–1780, https://doi.org/10.1016/j.cjph.2018.05.006.
[62] Y.L. Page, P. Saxe, Symmetry-general least-squares extraction of elastic coefficients from ab initio total energy calculations, Phys. Rev. B 63 (2001), 174103, https://doi.org/10.1103/PhysRevB.63.174103.
[63] H. Ozisik, E. Deligoz, K. Colakoglu, G. Surucu, Mechanical and lattice dynamical properties of the Re_2C compound, Phys. Status Solidi 4 (2010) 347–349, https://doi.org/10.1002/pssr.201004397.
[64] A. Shukoor V, M. Sarwan, S. Singh, Ground state structural, elastic, electronic properties and pressure-induced structural phase transition of XCoSb (X = Sc, Ti, V, Cr and Mn), J. Supercond. Nov. Magnetism 33 (2020) 1821–1829, https://doi.org/10.1007/s10948-020-05421-5.
[65] M. Born, K. Huang, Dynamical Theory of Crystal Lattices, Clarendon press, 1954.
[66] F. Mouhat, F.X. Coudert, Necessary and sufficient elastic stability conditions in various crystal systems, Phys. Rev. B 90 (2014), 224104, https://doi.org/10.1103/PhysRevB.90.224104.
[67] A. Erkisi, G. Surucu, R. Ellialtioglu, The investigation of electronic, mechanical and lattice dynamical properties of PdCoX (X = Si and Ge) half-Heusler metallics in α, β and γ structural phases: an ab initio study, Philos. Mag. A 97 (2017) 2237–2254, https://doi.org/10.1080/14786435.2017.1329595.
[68] D.C. Gupta, S. Ghosh, First-principal study of full Heusler alloys Co2VZ (Z = As, In), J. Magn. Magn Mater. 435 (2017) 107–116, https://doi.org/10.1016/j.jmmm.2017.03.067.
[69] W. Voigt, Lehrbuch der kristallphysik (The textbook of crystal physics), 1928 (Leipzig, Berlin, B.G. Teubner).
[70] A. Reuss, Berechnung der Fließgrenze von Mischkristallen auf Grund der Plastizitätsbedingung für Einkristalle, ZAMM - Zeitschrift Für Angew. Math. Und Mech. 9 (1929) 49–58, https://doi.org/10.1002/zamm.19290090104.
[71] R. Hill, The elastic behaviour of a crystalline aggregate, Proc. Phys. Soc. 65 (1952) 349–354, https://doi.org/10.1088/0370-1298/65/5/307.
[72] D.H. Wu, H.C. Wang, L.T. Wei, R.K. Pan, B.Y. Tang, First-principles study of structural stability and elastic properties of $MgPd_3$ and its hydride, J. Magnesium Alloys 2 (2014) 165–174, https://doi.org/10.1016/j.jma.2014.06.001.
[73] S.F. Pugh, XCII. Relations between the elastic moduli and the plastic properties of polycrystalline pure metals, Lond. Edinb. Dubl. Phil. Mag. 45 (1954) 823–843, https://doi.org/10.1080/14786440808520496.
[74] A. Erkisi, G. Surucu, The electronic and elasticity properties of new half-metallic chalcogenides Cu_3TMCh_4 (TM = Cr, Fe and Ch = S, Se, Te): an ab initio study, Philos. Mag. A 99 (2019) 513–529, https://doi.org/10.1080/14786435.2018.1546960.
[75] S. Akbudak, A. Candan, A.K. Kushwaha, M. Özduran, First principles investigation of the structural, elastic, electronic and vibrational properties of vanadium-based V3X (X = Fe, Co, and Ni) compounds, J. Phys. Chem. Solid. 150 (2021), 109854, https://doi.org/10.1016/j.jpcs.2020.109854.
[76] Y.O. Ciftci, M. Evecen, First principle study of structural, electronic, mechanical, dynamic and optical properties of half-Heusler compound LiScSi under pressure, Phase Transitions 91 (2018) 1206–1222, https://doi.org/10.1080/01411594.2018.1515433.
[77] X. Zhou, D. Gall, S.V. Khare, Mechanical properties and electronic structure of anti-ReO_3 structured cubic nitrides, M_3N, of d block transition metals M: an ab initio study, J. Alloys Compd. 595 (2014) 80–86, https://doi.org/10.1016/j.jallcom.2014.01.116.
[78] K. Lau, A.K. McCurdy, Elastic anisotropy factors for orthorhombic, tetragonal, and hexagonal crystals, Phys. Rev. B 58 (1998) 8980–8984, https://doi.org/10.1103/PhysRevB.58.8980.
[79] O.L. Anderson, A simplified method for calculating the debye temperature from elastic constants, J. Phys. Chem. Solid. 24 (1963) 909–917, https://doi.org/10.1016/0022-3697(63)90067-2.
[80] E. Schreiber, O.L. Anderson, N. Soga, Elastic Constants and Their Measurements, McGraw-Hill, New York, 1973.
[81] M.E. Fine, L.D. Brown, H.L. Marcus, Elastic constants versus melting temperature in metals, Scripta Metall. 18 (1984) 951–956, https://doi.org/10.1016/0036-9748(84)90267-9.
[82] G. Grimvall, Thermophysical Properties of Materials, Elsevier, North Holland, 1999.
[83] W. Qian, C. Zhang, Review of the phonon calculations for energetic crystals and their applications, Energetic Mater. Front. 2 (2021) 154–164, https://doi.org/10.1016/j.enmf.2021.03.002.
[84] F.T. Tahir, M. Husain, N. Sfina, A.A. Rached, M. Khan, N. Rahman, Probing the physical properties for prospective high energy applications of $QMnF_3$ (Q= Ga, In) halide perovskites compounds employing the framework of density functional theory, RSC Adv. 13 (2023) 18788–18798, https://doi.org/10.1039/D3RA02878J.
[85] D. Alfe, PHON: a program to calculate phonons using the small displacement method, Comput. Phys. Commun. 180 (2009) 2622–2633, https://doi.org/10.1016/j.cpc.2009.03.010.
[86] K. Parlinski, Z.Q. Li, Y. Kawazoe, First-principles determination of the soft mode in cubic ZrO2, Phys. Rev. Lett. 78 (1997) 4063, https://doi.org/10.1103/PhysRevLett.78.4063.
[87] H.B. Ozisik, K. Colakoglu, G. Surucu, H. Ozisik, Structural and lattice dynamical properties of Zintl NaIn and NaTl compounds, Comput, Mater. Sci. 50 (2011) 1070–1076, https://doi.org/10.1016/j.commatsci.2010.11.003.
[88] A.A. Maradudin, E.W. Montroll, G.H. Weiss, I.P. Ipatova, Theory of Lattice Dynamics in the Harmonic Approximation, Academic Press, New York and London, 1971.
[89] M.A. Blanco, E. Francisco, V. Luana, GIBBS: isothermal-isobaric thermodynamics of solids from energy curves using a quasi-harmonic Debye model, Comput. Phys. Commun. 158 (2004) 57–72, https://doi.org/10.1016/j.comphy.2003.12.001.
[90] S. Feng, S. Li, H. Fu, First-principle calculation and quasi-harmonic Debye model prediction for elastic and thermodynamic properties of Bi_2Te_3, Comput. Mater. Sci. 82 (2014) 45–49, https://doi.org/10.1016/j.commatsci.2013.09.037.